

Cite this: *Chem. Sci.*, 2018, 9, 8946

All publication charges for this article have been paid for by the Royal Society of Chemistry

Enhanced annihilation electrochemiluminescence by nanofluidic confinement†

Hanan Al-Kutubi,^{‡a} Silvia Voci,^{‡b} Liza Rassaei,^{cd} Neso Sojic^{id} ^{*b} and Klaus Mathwig^{id} ^{*a}

Microfabricated nanofluidic electrochemical devices offer a highly controlled nanochannel geometry; they confine the volume of chemical reactions to the nanoscale and enable greatly amplified electrochemical detection. Here, the generation of stable light emission by electrochemiluminescence (ECL) in transparent nanofluidic devices is demonstrated for the first time by exploiting nanogap amplification. Through continuous oxidation and reduction of $[\text{Ru}(\text{bpy})_3]^{2+}$ luminophores at electrodes positioned at opposite walls of a 100 nm nanochannel, we compare classic redox cycling and ECL annihilation. Enhanced ECL light emission of attomole luminophore quantities is evidenced under ambient conditions due to the spatial confinement in a 10 femtoliter volume, resulting in a short diffusion timescale and highly efficient ECL reaction pathways at the nanoscale.

Received 19th July 2018
Accepted 30th September 2018

DOI: 10.1039/c8sc03209b

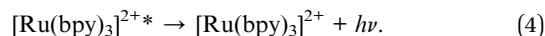
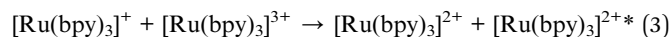
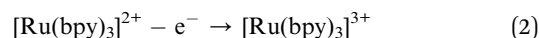
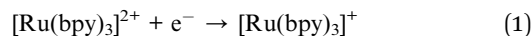
rsc.li/chemical-science

Introduction

Electrochemiluminescence (ECL) is the emission of light by electrochemical means: reactive species are generated at the electrode surface and undergo a highly exergonic electron-transfer reaction producing the excited state of the luminophore.¹ It relaxes to the ground state, emitting a photon. The possibility to regenerate the reactive species *in situ* as well as not requiring an external light source for excitation, gives this method many advantages for (bio)sensing applications, single object imaging,^{2–4} and light-emitting devices.⁵ These advantages include a straightforward experimental setup, a very high sensitivity and a wide detection range. Thus, applications and fundamental aspects of ECL have been researched extensively.⁵

Whereas the precise mechanism of light generation depends on the species involved, there are two dominant pathways: the annihilation and the co-reactant pathways.¹ Here, we focus on the annihilation pathway in a nanochannel, in which light is generated through a reaction between the oxidized and reduced forms of the original compound. We selected tris(bipyridine)

ruthenium(II), $[\text{Ru}(\text{bpy})_3]^{2+}$, one of the most well-studied ECL compounds^{6,7} due to its relatively high quantum yield, water solubility and long-lived triplet excited state. Its annihilation pathway is:⁸



These reactions were initially investigated by rapidly pulsing a single electrode between the oxidizing and reducing potential.^{9,10} However, this technique suffers from drawbacks¹¹ such as large charging currents. Using two electrodes, both $[\text{Ru}(\text{bpy})_3]^+$ and $[\text{Ru}(\text{bpy})_3]^{3+}$ can be generated in close vicinity under steady-state conditions. Various two-electrode setups have been employed, including ring and disk electrodes,¹² thin layer cells,¹³ band electrodes,^{14–16} and scanning electrochemical microscopy.^{17,18} These studies have shown that annihilation occurs more efficiently at smaller inter-electrode distances^{16,18} as the diffusional distance between electrogenerated $[\text{Ru}(\text{bpy})_3]^+$ and $[\text{Ru}(\text{bpy})_3]^{3+}$ is decreased. Indeed, the stability of the reduced form, $[\text{Ru}(\text{bpy})_3]^+$, is a key issue limiting the efficiency of the annihilation ECL. Yet, observation of light emission so far has been limited to a minimum inter-electrode distance of 2 μm .^{18,19} In addition, due to the sensitivity of annihilation ECL towards impurities such as dioxygen and water, experiments are performed in drastic conditions: dried and distilled solvents just before use, recrystallized and dried luminescent compounds and supporting electrolytes, under an inert

^aUniversity of Groningen, Groningen Research Institute of Pharmacy, Pharmaceutical Analysis, P.O. Box 196, 9700 AD Groningen, The Netherlands. E-mail: kmathwig@rug.nl

^bUniversity of Bordeaux, Bordeaux INP, Institut des Sciences Moléculaires, UMR CNRS 5255, 33607 Pessac, France. E-mail: neso.sojic@enscbp.fr

^cRotterdam School of Management, Erasmus University, Burgemeester Oudlaan 50, 3062 PA Rotterdam, The Netherlands

^dDelft University of Technology, Van der Maasweg 9, 2629 HZ Delft, The Netherlands

† Electronic supplementary information (ESI) available: Chemical reagents, device fabrication, background measurement, and finite element modeling, numerical concentration profiles. See DOI: 10.1039/c8sc03209b

‡ These authors contributed equally.



ECL-emission is produced in annihilation mode inside a nanochannel and was imaged and spatially resolved as shown in Fig. 3 using an epifluorescence microscope (DMI6000, Leica). Photon emission was collected by an inverted 40 \times microscope objective and detected by an Electron Multiplying Charge Coupled Device (EM-CCD) Camera (Hamamatsu, 9100-13). Light emission from a luminophore quantity of 60 attomoles present in the active area of the device was intense enough to be recorded through the 20 nm-thick semi-transparent Pt bottom electrode, due to nanogap amplification. The overlay image (Fig. 3a, right) shows that ECL intensity is uniform along the channel and decreases rapidly at the edges. No emission is seen from the bottom electrode area under the access holes. Furthermore, ECL emission is limited to a region narrower than the 5 μm wide channel. This indicates that emission is caused exclusively by reaction in the 3 μm \times 20 μm effective area between the electrodes (as observed for purely electrochemical cycling³⁰). Full-width-at-half-maxima of longitudinal and lateral intensity profiles amount to 20 μm and 4.3 μm , respectively. Presumably, the optical resolution of the 40 \times objective as well as inhomogeneous transparency of Pt and glass lead to a slightly wider profile than expected. Clearly, ECL emission is confined to the active area of the nanochannel, where reactions (1–4) (Fig. 2b) take place.

The constant ECL intensity along the nanochannel (Fig. 3b, blue curve) indicates that only negligible degradation occurs. If $[\text{Ru}(\text{bpy})_3]^+$ or $[\text{Ru}(\text{bpy})_3]^{3+}$ would degrade, the intensity would be strongly attenuated in the center of the channel because the chance of encountering contaminants increases quadratically as luminophores diffuse towards the center.

Fig. 4a displays the chronoamperometric currents at both electrodes when stepping between redox cycling and

annihilation ECL modes. In redox cycling mode, the oxidation and reduction currents are symmetric and constant. The observed currents of ~ 0.65 μA are in agreement with an expected analytical estimate³¹ of $I_{\text{lim}} = \frac{FADc}{h} = 0.58$ μA (F : faraday constant; A : active area of 3 μm by 20 μm ; $D = 1 \times 10^{-9}$ $\text{m}^2 \text{s}^{-1}$ diffusion coefficient, c : 10 mM $[\text{Ru}(\text{bpy})_3]^{2+}$ concentration, h : 100 nm channel height).

ECL intensity was measured simultaneously by using a photomultiplier tube (Hamamatsu R4632). The signal was amplified by a Keithley Picoammeter before acquisition with the second input signal of a $\mu\text{Autolab}$ type II potentiostat. Emission was not observed in redox cycling mode (Fig. 4b). Upon switching to annihilation mode, an initial transient current increase can be ascribed to adsorption of analytes onto the electrode surfaces due to the high surface-to-volume ratio of the nanogap devices.^{22,29,32} Oxidation and reduction currents are symmetric as expected for reactions (1–4). In annihilation mode, the light intensity (Fig. 4b) exhibits a strong transient behavior before approaching a steady state. Understanding this transient behavior will require further studies, we partially attribute the complex transient to desorption when stepping the potential as well as accumulating $[\text{Ru}(\text{bpy})_3]^{3+}$ during redox cycling.

Upon switching from redox cycling to annihilation mode, an expected increase in the current is observed as the diffusive path for cycling molecules halves to 50 nm. Concentration profiles of all $[\text{Ru}(\text{bpy})_3]$ species are illustrated in Fig. 5 (COM-SOL Multiphysics, see ESI[†]). Considering the symmetry of the nanofluidic channel and the annihilation reaction (*i.e.*, double cycling redox process), ECL is emitted in the middle of the



Fig. 3 (a) From left to right: bright-field micrograph of the nanochannel, ECL emission recorded in the dark, and overlay of both images (dashed lines: direction of profiles in (b)). (b) ECL intensity profiles along (blue) and across (orange) the center of the channel, using a solution of 10 mM $\text{Ru}(\text{bpy})_3(\text{PF}_6)_2$ and 0.1 M TBAPF_6 in acetonitrile. The top electrode was biased at 2 V, the bottom electrode at -1.5 V vs. Ag.



Fig. 4 (a) Measured chronoamperometric currents at the top (blue) and bottom (green) electrodes, and (b) corresponding ECL intensity. The top electrode was maintained at 2.3 V while the bottom electrode was pulsed between 0 V and -1.5 V vs. Ag, highlighted in white (redox cycling mode) and grey (annihilation ECL mode), respectively. Solution consisted of 10 mM $\text{Ru}(\text{bpy})_3(\text{PF}_6)_2$ and 0.1 M TBAPF_6 in acetonitrile.



- 11 F. F. Fan, in *Electrogenerated Chemiluminescence*, ed. A. J. Bard, CRC Press, New York, 1st edn, 2004, pp. 23–99.
- 12 J. T. Maloy, K. B. Prater and A. J. Bard, *J. Am. Chem. Soc.*, 1971, **93**, 5959–5968.
- 13 G. H. Brilmyer and A. J. Bard, *J. Electrochem. Soc.*, 1980, **127**, 104–110.
- 14 J. E. Bartelt, S. M. Drew and R. M. Wightman, *J. Electrochem. Soc.*, 1992, **139**, 70–74.
- 15 C. Amatore, C. Pebay, L. Servant, N. Sojic, S. Szunerits and L. Thouin, *ChemPhysChem*, 2006, **7**, 1322–1327.
- 16 G. C. Fiaccabrino, M. Koudelka-Hep, Y. T. Hsueh, S. D. Collins and R. L. Smith, *Anal. Chem.*, 1998, **70**, 4157–4161.
- 17 F.-R. F. Fan, D. Cliffel and A. J. Bard, *Anal. Chem.*, 1998, **70**, 2941–2948.
- 18 J. Rodríguez-López, M. Shen, A. B. Nepomnyashchii and A. J. Bard, *J. Am. Chem. Soc.*, 2012, **134**, 9240–9250.
- 19 M. Shen, N. Arroyo-Currás and A. J. Bard, *Anal. Chem.*, 2011, **83**, 9082–9085.
- 20 A. Kapturkiewicz and G. Angulo, *Dalton Trans.*, 2003, 3907–3913.
- 21 M. A. G. Zevenbergen, D. Krapf, M. R. Zuiddam and S. G. Lemay, *Nano Lett.*, 2007, **7**, 384–388.
- 22 D. Mampallil, K. Mathwig, S. Kang and S. G. Lemay, *J. Phys. Chem. Lett.*, 2014, **5**, 636–640.
- 23 Q. Chen, K. McKelvey, M. A. Edwards and H. S. White, *J. Phys. Chem. C*, 2016, **120**, 17251–17260.
- 24 C. Ma, W. Xu, W. R. A. Wichert and P. W. Bohn, *ACS Nano*, 2016, **10**, 3658–3664.
- 25 L. Rassaei, K. Mathwig, S. Kang, H. A. Heering and S. G. Lemay, *ACS Nano*, 2014, **8**, 8278–8284.
- 26 S. Kang, A. F. Nieuwenhuis, K. Mathwig, D. Mampallil, Z. Kostiuhenko and S. G. Lemay, *Faraday Discuss.*, 2016, **193**, 41–50.
- 27 D. Han, G. M. Crouch, K. Fu, L. P. Zaino III and P. W. Bohn, *Chem. Sci.*, 2017, **8**, 5345–5355.
- 28 K. Mathwig and S. G. Lemay, *Micromachines*, 2013, **4**, 138–148.
- 29 S. Kang, K. Mathwig and S. G. Lemay, *Lab Chip*, 2012, **12**, 1262–1267.
- 30 S. Kang, A. F. Nieuwenhuis, K. Mathwig, D. Mampallil and S. G. Lemay, *ACS Nano*, 2013, **7**, 10931–10937.
- 31 D. Mampallil, K. Mathwig, S. Kang and S. G. Lemay, *Anal. Chem.*, 2013, **85**, 6053–6058.
- 32 E. Kätelhön, K. J. Krause, K. Mathwig, S. G. Lemay and B. Wolfrum, *ACS Nano*, 2014, **8**, 4924–4930.
- 33 Q. Wang, J. Rodríguez-López and A. J. Bard, *ChemPhysChem*, 2010, **11**, 2969–2978.
- 34 C. Amatore, F. BonhSomme, J. L. Bruneel, L. Servant and L. Thouin, *J. Electroanal. Chem.*, 2000, **484**, 1–17.
- 35 M. M. Collinson, R. M. Wightman and P. Pastore, *J. Phys. Chem.*, 1994, **98**, 11942–11947.

